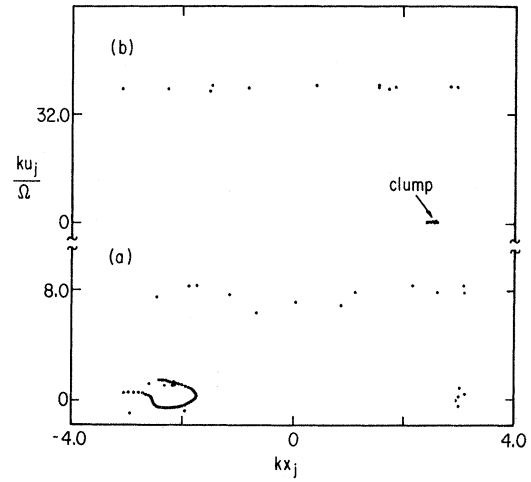

FIG. 4. Phase-space plot showing the formation of a singular charge clump; $E_0=0.5$, $\Gamma=0.05$, (a) $\tau=25.0$, (b) $\tau=85.0$.

In summary, the present study shows that when the exact beam dynamics are followed it is possible for a runaway beam to become clamped. This result confirms an earlier prediction[7] of this effect based on a spatially averaged formalism. The clamping process generates a runaway wave, thus suggesting an efficient method[8] for converting dc to ac energy. When wave damping is present, a dynamic BGK equilibrium is approached in which the beam evolves into a singular charge clump that drifts through the plasma at constant velocity. The stability and limiting factors of this state require further study.

The author thanks Dr. G. Dimonte, J. N. Leboeuf, and T. Tajima for useful conversations on this topic. This work was supported by the U. S. Office of Naval Research and by the U. S. Department of Energy, Contract No. EY-76-C-03-0010 PA26.

[1]T. M. O'Neil, J. H. Winfrey, and J. H. Malmberg, Phys. Fluids 14, 1204 (1971).

[2]I. N. Onishchenko, A. R. Liveskii, M. C. Matsiborko, V. D. Shapiro, and V. I. Shevchenko, Pis'ma Zh. Eksp. Teor. 12, 407 (1970) [JETP Lett. 12, 281 (1970)].

[3]K. W. Gentle and J. Lohr, Phys. Fluids 16, 1464 (1973).

[4]G. Dimonte and J. H. Malmberg, Phys. Fluids 21, 1188 (1978).

[5]I. B. Bernstein, J. Greene, and M. D. Kruskal, Phys. Rev. 108, 546 (1957).

[6]Of course, the system can also be satisfied by having both states simultaneously, i.e., some of the beam particles run away while others remain clamped, as seen in Fig. 4. This transition region is expected to predominate as E_0 approaches E_T.

[7]G. J. Morales and Y. C. Lee, Bull. Am. Phys. Soc. 22, 1173 (1977), and University of California at Los Angeles, Plasma Physics Group, Report No. PPG-358, June 1978 (unpublished).

[8]The ac enhancement and the existence of a collective runaway threshold have been found also in a relativistic particle simulation, J. N. Leboeuf, T. Tajima, and G. J. Morales, University of California at Los Angeles, Plasma Physics Group, Report No. PPG-349, April 1978 (unpublished).

Theory of Universal Eigenmodes in a Sheared Magnetic Field

Liu Chen, P. N. Guzdar, R. B. White, P. K. Kaw, and C. Oberman
Plasma Physics Laboratory, Princeton University, Princeton, New Jersey 08540

(Received 17 May 1978)

Collisionless drift-wave eigenmodes in a sheared magnetic field are analyzed using the WKBJ method. It is found that, for $L_s/L_n > (L_s/L_n)_c$, ion-sound dynamics determines the eigenvalues at small k_y^2 and the eigenmodes are damped. However, at large k_y^2, electron dynamics dominates and the eigenmodes become marginally stable. For $L_s/L_n < (L_s/L_n)_c$, the eigenmodes are damped for all values of k_y^2. The critical value $(L_s/L_n)_c$ scales as $(m_i/m_e)^{1/4}$.

Recently, Ross and Mahajan[1] as well as Tsang *et al.*[2] have made an important contribution to the theory of collisionless drift-wave eigenmodes in a slab geometry with finite magnetic shear. In contradiction to previous theoretical predictions,[3] they found numerically that, with *full* (both resonant and nonresonant) electron dynamics taken into account, there is *no* absolutely unstable drift wave. They point out that the errors in previous theories are due to retaining only resonant electron dynamics and/or using improper perturbation analyses.

While the numerical results obtained by these authors appear correct, their analytical theories seem dubious. Specifically, in Ref. 1, the authors employed a variational principle to derive the eigenvalue condition. The eigenvalue condition thus derived depends critically on the integral

$$I=\int_{-\infty}^{\infty} dx\, \varphi^2 Z(x_e/|x|)/|x|,$$

where $x_e=\omega L_s/k_y v_e$, Z is the plasma dispersion function,[4] and $\varphi(x)$ is a trial function chosen to be $\exp(-i\alpha x^2/2)$. Contrary to what the authors have assumed [cf. their Eq. (8)], however, we note that α always contains a positive imaginary part and, therefore, the integral I tends to be divergent. In fact, the divergence of I is much more severe at larger k_y^2 where the modes are marginally stable and the corresponding α values are purely positive imaginary! (We have confirmed this by independent numerical work.) Thus, at least for the marginally stable modes the analysis is inconsistent. In Ref. 2, the eigenvalue problem was solved by the method of matched asymptotic expansions. In the outer region ($|x|>|x_e|$), the authors neglected the electron Z function and, with the outgoing-wave boundary condition, obtained a solution in terms of parabolic cylinder functions. The eigenvalue condition was then derived by matching the slope φ'/φ of the outer-region solution to that of the inner-region solution using the electron Z function and the "constant-φ" approximation. However, in evaluating the inner-region φ'/φ, only the resonant electron contributions [cf. the logarithmic term in their Eq. (2)] are included! This contradicts their numerical work which indicates that it is necessary to retain the full electron dynamics to obtain marginal stability. Thus, it is not all clear why this calculation agrees with their numerical work. Recently, Antonsen[5] has shown the nonexistence of absolutely unstable eigenmodes. His work, however, by its very nature, cannot describe the weakly damped or marginally stable modes. Since such modes, by convective amplification,[6,7] can still be dangerous to plasma confinement, it is important to understand their properties in detail.

In this Letter we present an eigenmode analysis employing the WKBJ or phase-integral method.[8] The WKBJ approach is motivated by the large parameter, L_s/L_n. We find that there exists a critical shear scale length, $(L_s/L_n)_c$. For $L_s/L_n<(L_s/L_n)_c$, i.e., strong shear, the eigenvalues are determined by the turning points due to the ion-sound waves (i.e., the Pearlstein-Berk turning points)[3] and eigenmodes are found to be damped for all k_y^2. For $L_s/L_n>(L_s/L_n)_c$, i.e., weak shear, there is a critical perpendicular wave number, k_{yc}^2. At long wavelengths, $k_y^2<k_{yc}^2$, the Pearlstein-Berk turning points again determine the eigenvalues and there are only damped eigenmodes. For $k_y^2>k_{yc}^2$, however, we find that the eigenvalues are determined by a new pair of turning points induced by the electron dynamics and, in this case, the eigenmodes are predicted to be marginally stable. For this parameter range, it can be expected that the analytical theories of Refs. 1 and 2 do not properly describe the marginally stable eigenmodes because both the trial function $\varphi=\exp(-i\alpha x^2/2)$ and the "constant-φ" approximation assumed implicitly that the Pearlstein-Berk turning points determine the eigenmodes.

Let us consider, for simplicity, cold ions and no temperature gradients. The corresponding eigenmode equation is given by

$$[d^2/dx^2+Q(x)]\varphi(x)=0, \tag{1}$$

where

$$Q(x)=\lambda+x^2/4+(\mu\epsilon/|x|)Z(\epsilon/|x|), \tag{2}$$

$$\lambda=-(\omega L_s/2\omega_* L_n)(k_y^2\rho_s^2+1-\omega_*/\omega), \tag{3}$$

$$\mu=(L_s/2L_n)(1-\omega/\omega_*), \tag{4}$$

$$\epsilon=(\omega m_e L_s/\omega_* m_i L_n)^{1/2}, \tag{5}$$

and the rest of the notations are standard. The analytical continuation of this expression into the complex plane $t=x+iy$ is provided by $|x|\to(t^2)^{1/2}$. The Riemann structure consists of two cuts originating at $t=0$, which we take along the positive and negative imaginary axes, respectively. There are two sheets, which we refer to as the physical sheet, $(x^2)^{1/2}>0$, and the nonphysical sheet, $(x^2)^{1/2}<0$.

There are three pairs of turning points in the complex t plane, each pair being symmetrically located about the origin. The first pair corresponds to the usual ion-sound (Pearlstein-Berk) turning points:

$$\pm P\simeq\mp(2i\lambda^{1/2}-i\pi^{1/2}\mu\epsilon/2\lambda). \tag{6}$$

The second pair, which also plays a role in the WKBJ analysis, is induced by the electron dynamics via the Z function and its location is approximately given by

$$\pm E\simeq\mp i\pi^{1/2}\mu\epsilon/\lambda. \tag{7}$$

The third pair normally is found further out in the complex plane and plays no essential role in the WKBJ analysis. Its appropriate location is given by

$$\pm B \simeq \mp(2i\lambda^{1/2} + i\pi^{1/2}\mu\epsilon/2\lambda). \quad (8)$$

In deriving Eqs. (6) to (8), we have assumed that $|\mu\pi^{1/2}| > |\lambda|$ and $|2\lambda^{3/2}| > |\pi^{1/2}\mu\epsilon|$, which are usually satisfied. We note also that $\pi/2 > \arg(\lambda) \geq 0$ and, since $|\omega_r| \gg |\omega_i|$, μ and ϵ are predominantly real.

For small k_y^2 we have $\arg(\lambda) > 0$. $\pm P$ are located in the fourth and second quadrants of the physical sheet, respectively. $\pm B$ and $\pm E$ are on the nonphysical sheet. The corresponding Stokes diagram is shown in Fig. 1. For this Stokes pattern the outgoing-wave boundary condition at large $|x|$ corresponds to taking dominant solutions (with respect to $\pm P$) in regions (i) and (i)′ and, hence, subdominant solutions in (ii) and (ii)′. The eigenvalue condition is then determined by the physical Pearlstein-Berk turning point; i.e.,

$$\int_0^P [Q(t)]^{1/2} dt = (2n+1)\pi/4; \; n = 0, 1 \ldots . \quad (9)$$

The Stokes diagrams and eigenvalues presented here have been determined by a code which uses the eigenvalue condition [e.g., Eq. (9)] to search iteratively the complex frequency plane. Once the frequency has been determined, the resulting Stokes diagram indicates the possible choices of boundary conditions for the solution.[5] We note that, for the present case of small k_y^2, the eigenmodes are found to be damped. As k_y^2 is increased, $\arg(\lambda)$ decreases and all three pairs of turning points migrate toward the imaginary (y) axis. (This tendency can be readily seen using a perturbation theory.) The properties of the eigenvalue problem, however, depend critically on whether the magnetic shear is weak or strong.

In the weak-shear case, $L_s/L_n > (L_s/L_n)_c$, there exists a critical value of k_y^2, k_{yc}^2, at which the Pearlstein-Berk pair $\pm P$ and the electron-induced pair $\pm E$ *coalesce* at $\pm C$. The value of k_{yc}^2 can be determined by the coalescence conditions $Q(C) = Q'(C) = 0$, and the eigenvalue condition $\int_0^C [Q(t)]^{1/2} \times dt = (2n+1)\pi/4$. In the present analysis, k_{yc}^2 depends on m_e/m_i and L_n/L_s. For example, with $m_i/m_e = 1837$, we find $k_{yc}^2\rho_s^2 = 0.13$ for $L_s/L_n = 50$ and $k_{yc}^2\rho_s^2 = 0.045$ for $L_s/L_n = 100$. We note that C lies on the imaginary (y) axis. Since $Z(iv) = i\pi^{1/2}\exp(v^2)\operatorname{erfc}(v)$,[4] it then easily follows that $\mathrm{Im}\omega = 0$ and the eigenmode is marginally stable.

As k_y^2 is increased beyond k_{yc}^2, P and E again separate. All three pairs of turning points stay, however, on the imaginary axis. With increasing k_y^2, E slowly migrates toward the origin and P and B move in the opposite direction. The Stokes diagram corresponding to this regime of large k_y^2 is shown in Fig. 2. Again, the outgoing-wave boundary condition along x dictates that the solutions be dominant in regions (i) and (i)′ and, thus, subdominant in (ii) and (ii)′. Therefore, the ei-

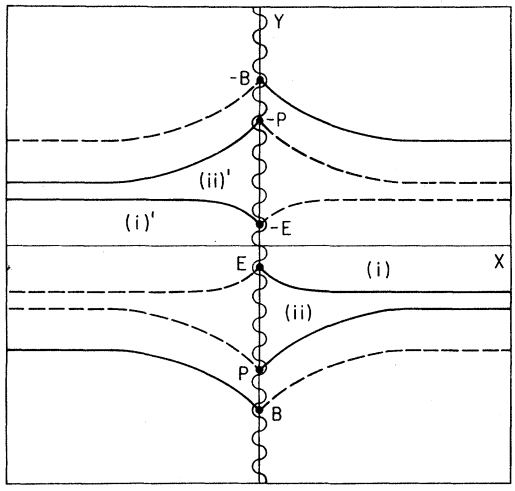

FIG. 1. Stokes diagram for the case with $k_y^2 < k_{yc}^2$, i.e., damped eigenmodes. The solid (dashed) lines are anti-Stokes on the physical (nonphysical) sheet. The wavy line is the branch cut.

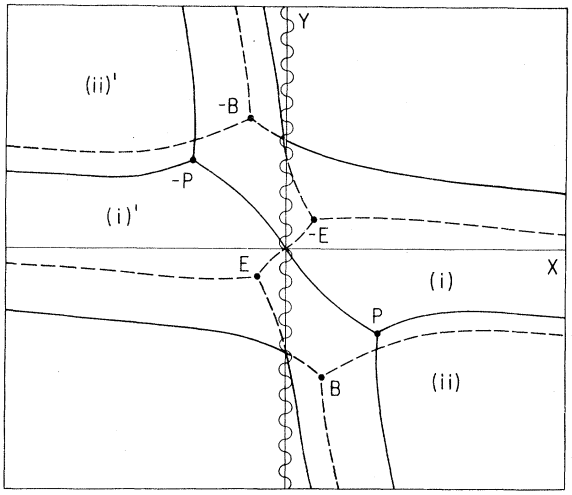

FIG. 2. Stokes diagram for the case with $k_y^2 > k_{yc}^2$, i.e., marginally stable eigenmodes. The rest is the same as in Fig. 1.

genvalue condition is determined by E instead of P; i.e., we have

$$\int_0^E [Q(t)]^{1/2}\,dt=(2n+1)\pi/4;\quad n=0,1.\ldots \qquad (10)$$

Since E lies on the y axis, the eigenmodes continue to be marginally stable. Here, we should remark that while the full Z function is well behaved along the y (imaginary) axis, the resonant-electron contribution alone, $i\pi^{1/2}\exp[-\omega^2/(k_\parallel{}'^2 \times v_e{}^2t^2)]$, is not. Thus, the coalescence of turning points as well as the eigenvalue condition, Eq. (10), is pertinent to the case with the full electron dynamics included.

In the strong-shear case, $L_s/L_n<(L_s/L_n)_c$, however, P and E do not *coalesce* for any value of $k_y{}^2$. The corresponding Stokes diagram is similar to that shown in Fig. 1. The eigenvalue condition is then given by Eq. (9) and the eigenmodes are damped for all $k_y{}^2$. We note that, in the present analysis, $(L_s/L_n)_c$ is a function of m_i/m_e only. We have computed $(L_s/L_n)_c$ for the $n=0$ eigenmode and a wide range of m_i/m_e. The results are shown in Fig. 3 using a log-log plot. Interestingly, the results indicate that $(L_s/L_n)_c$ scales as $(m_i/m_e)^{1/4}$. In fact, the following is a closely fitting scaling law:

$$(L_s/L_n)_c=3(m_i/m_e)^{1/4}. \qquad (11)$$

Here, it is interesting to contrast the scaling law of $(L_s/L_n)_c$ given by Eq. (11) with the $(m_i/m_e)^{1/3}$ scaling of L_s/L_n found in previous perturbative[3] and convective amplification treatments.[6]

The WKBJ results presented here have also been verified by direct numerical integration of Eq. (1). Taking $m_i/m_e=1837$ and $L_s/L_n=50$, and using the WKBJ eigenvalue conditions [Eqs. (9) and (10)], we have computed ω of the $n=0$ eigenmode for a range of $k_y{}^2$. Figure 4 shows the analytical (WKBJ) results as well as those

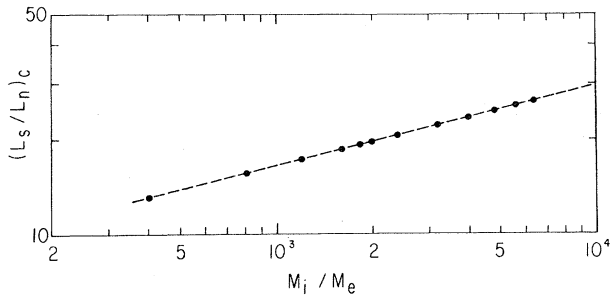

FIG. 3. A log-log plot of $(L_s/L_n)_c$ vs m_i/m_e.

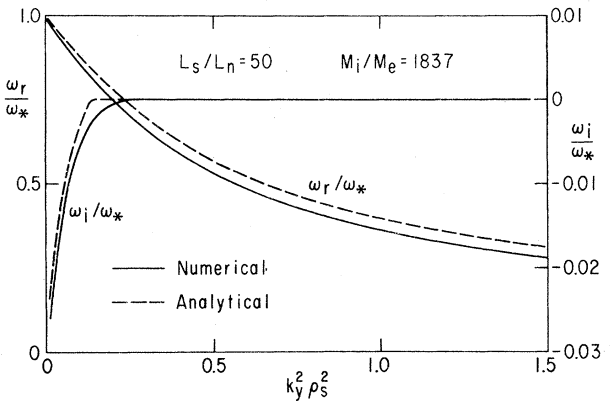

FIG. 4. Plot of ω_r and ω_i vs $k_y{}^2\rho_s{}^2$.

obtained numerically using a shooting scheme (identical to that in Ref. 1. The agreement is sufficiently good. We have also examined the case with $L_s/L_n=100$ and obtained better agreement, as is expected because the WKBJ approximation becomes better as the large parameter L_s/L_n increases. Finally, we have also confirmed numerically that for $L_s/L_n<(L_s/L_n)_c$ there is no transition to a marginally stable mode; the eigenmodes are always damped. Using a value of $L_s/L_n=10$, which is less than the critical value of $(L_s/L_n)_c\simeq 19$ $(m_i/m_e=1837)$, we have run the numerical shooting code for $k_y{}^2$ up to a large value, $k_y{}^2\rho_s{}^2=20$. Throughout this entire range, the $n=0$ eigenmode remains damped and the damping rate asymptotically approaches a constant value.

In conclusion, we have shown that *only* for sufficiently weak shear $L_s/L_n>(L_s/L_n)_c\sim(m_i/m_e)^{1/4}$, do the collisionless drift-wave eigenmodes become marginally stable for large $k_y{}^2$. (In the opposite limit, the modes are always damped.) An interesting consequence might be that for $L_s/L_n>(L_s/L_n)_c$, convective amplification of noise perturbations in the plasma could be enormous and limited only by nonlinear effects.

This paper is jointly supported by U. S. Department of Energy Contract No. EY-76-C-02-3073 and by U. S. Air Force Office of Scientific Research Contract No. F 44620-75-C-0037.

[1]D. W. Ross and S. M. Mahajan, Phys. Rev. Lett. 40, 324 (1978).

[2]K. T. Tsang, P. J. Catto J. C. Whitson, and J. Smith, Phys. Rev. Lett. 40, 327 (1978).

[3]L. D. Pearlstein and H. L. Berk, Phys. Rev. Lett.

23, 220 (1969); N. T. Gladd and W. Horton, Jr., Phys. Fluids 16, 879 (1973); M. N. Rosenbluth and P. J. Catto, Nucl. Fusion 15, 573 (1975).

[4]B. D. Fried and S. D. Conte, *The Plasma Dispersion Function* (Academic, New York, 1961).

[5]T. M. Antonsen, Jr., Phys. Rev. Lett. 41, 33 (1978).

[6]P. H. Rutherford and E. A. Frieman, Phys. Fluids 10, 1007 (1967).

[7]B. Coppi, G. Laval, R. Pellat, and M. N. Rosenbluth, Nucl. Fusion 6, 261 (1966).

[8]J. Heading, *An Introduction to Phase Integral Methods* (Wiley, New York, 1962); R. B. White, Princeton University Plasma Physics Laboratory Report No. PPPL-1428, 1978 (unpublished).

Magnetostatic Mode and Cross-Field Electron Transport

Cheng Chu, Ming-Sheng Chu, and Tihiro Ohkawa
General Atomic Company, San Diego, California 92138

(Received 25 April 1978)

A zero-frequency magnetostatic mode is shown to exist in a magnetized plasma. This mode resembles the two-dimensional electrostatic convective-cell mode in many ways. Electron cross-field test-particle diffusion due to thermally excited magnetostatic modes exhibits the Bohm-like T/B behavior. This mode would enhance the electron heat and momentum transport and could permit rapid spreading of plasma current.

Since the discovery of the zero-frequency electrostatic convective-cell (vortex) mode[1] in two-dimensional plasma, remarkable advances have been made on the theory of plasma transport by collective processes.[2-5] It has been demonstrated, both computationally and analytically, that even for a plasma in thermal equilibrium the long-lived, large-scale, low-frequency fluctuating electric field can cause convection of the plasma by $\vec{E}\times\vec{B}$ drifts across the externally applied confining magnetic field and thus cause cross-field plasma transport well above the classical collisional value. Evidence of plasma transport by convective cells has also been observed experimentally.[6,7] In this paper, we show that besides the electrostatic convective cell, a zero-frequency magnetostatic mode can also exist in a magnetized plasma. In the plane perpendicular to the externally applied static magnetic field, the particle motion (resulting from streaming along the perturbed magnetic field line) of this mode resembles that of the $\vec{E}\times\vec{B}$ motion of the convective cell. Similar to the convective cell, the long-wavelength magnetostatic mode can persist for a long time. The cross-field test-particle diffusion from thermally excited magnetostatic modes exhibits the Bohm-like T/B scaling.

For a uniform plasma immersed in a constant magnetic field $\vec{B}_0 = B_0\hat{z}$ there are two types of modes which can propagate across the ambient magnetic field ($k_z = 0$): (1) the extraordinary mode[8] with dispersion relation $N^2 = RL/S$ and (2) the ordinary mode[8] with dispersion relation $N^2 = P$ (the notations are the same as those defined in Ref. 8). Electrostatic waves are a subset of the extraordinary mode in the limit that N^2 approaches infinity ($S \to 0$), and the convective cell is one of them. The second type of mode, the ordinary mode, is a purely transverse electromagnetic wave: The wave vector, the wave electric field (which is parallel to the external magnetic field), and the wave magnetic field form a right-handed orthogonal set, while the charge-density variation is zero and only the $\hat{z}$ component of the vector potential $\vec{A}$ is involved. As we will show below, a zero-frequency mode similar to the electrostatic convective cell exists in this type of transverse electromagnetic wave. The technique developed in Ref. 3 can be used here; however, because of the complexity of the mathematics involved, it seems more appropriate to use a heuristic approach instead. The equations to be used in the analysis are the wave equation for the perturbation A_z,

$$\nabla^2 A_z - \frac{1}{c^2}\frac{\partial^2 A_z}{\partial t^2} = -\frac{4\pi}{c} j_z, \tag{1}$$

and the electron momentum equation in the z direction,

$$\partial v_z/\partial t + \vec{v}\cdot\nabla v_z = -(q/m)E_z + \mu\nabla^2 v_z - \nu v_z, \tag{2}$$

where c is the speed of light, ν is the electron-ion collision frequency, and μ is the collective shear viscosity[9] which will be calculated later when we consider the particle motion in the plane perpendicular to $\hat{z}$. Because of their consider-